Empirical model of nitric oxide in the lower thermosphere

D. R. Marsh and S. C. Solomon
National Center for Atmospheric Research, Boulder, Colorado, USA

A. E. Reynolds
Department of Meteorology, Pennsylvania State University, University Park, Pennsylvania, USA

Received 19 August 2003; revised 19 February 2004; accepted 26 April 2004; published 7 July 2004.

[1] The Student Nitric Oxide Explorer (SNOE) satellite made near-continuous measurements of nitric oxide in the lower thermosphere (97.5 km to 150 km) between March 1998 and September 2000. Using eigenanalysis, this daily nitric oxide data set is represented as a time mean plus the sum of orthogonal functions of space multiplied by time-varying coefficients. The functions, typically called empirical orthogonal functions (EOFs), are ordered by the amount of variance they capture from the original data set. While this analysis in no way guarantees that the modes of variability identified by the EOFs are associated with physical processes, we show that it is clearly so for the first three EOFs of the SNOE data set. The dominant mode of variability is associated with auroral activity, followed by a seasonal effect, and then a response to varying solar EUV flux. As a result, it is possible to construct a compact, three-dimensional nitric oxide empirical model (NOEM) in the lower thermosphere that takes as input a planetary magnetic index, day of year, and 10.7 cm solar radio flux. Since it is possible that changes in lower thermospheric nitric oxide could lead to changes in stratospheric ozone, the model presented here can be utilized in climate simulations without the need to incorporate many thermospheric processes. *INDEX TERMS:* 0355 Atmospheric Composition and Structure: Thermosphere—composition and chemistry; 0358 Atmospheric Composition and Structure: Thermosphere—energy deposition; 1650 Global Change: Solar variability; 0310 Atmospheric Composition and Structure: Airglow and aurora; 2704 Magnetospheric Physics: Auroral phenomena (2407); *KEYWORDS:* nitric oxide, lower thermosphere, empirical models, SNOE

Citation: Marsh, D. R., S. C. Solomon, and A. E. Reynolds (2004), Empirical model of nitric oxide in the lower thermosphere, *J. Geophys. Res.*, *109*, A07301, doi:10.1029/2003JA010199.

1. Introduction

[2] The study of nitric oxide (NO) in the upper atmosphere is interesting for several reasons. First, NO in the lower thermosphere is known to vary considerably with solar and auroral activity. This was observed, for example, in measurements made between 1981 and 1986 by the Solar Mesosphere Explorer satellite [*Barth et al.*, 1988; *Siskind et al.*, 1989a, 1989b; *Gerard et al.*, 1990; *Fuller-Rowell*, 1993; *Barth*, 1996]. In those observations, low-latitude NO variations were clearly correlated with the highly variable solar soft X-ray fluxes [*Barth et al.*, 1988]. More recently, Student Nitric Oxide Explorer (SNOE) measurements of NO by the gamma-band fluorescence technique, along with simultaneous solar flux observations between 2 and 10 nm, confirmed that the low-latitude variability of NO was primarily the result of variations in solar soft X-ray emissions [*Barth et al.*, 1999]. In addition, SNOE NO observations at geomagnetic latitudes greater than 50° showed NO variations were highly correlated with auroral activity [*Solomon et al.*, 1999]. Second, emission at 5.3 μm from NO is an important cooling mechanism in the thermosphere. *Richards et al.* [1982] calculated that NO cooling decreases the heating efficiency near 130 km by approximately a factor of 4 in the summer hemisphere. As a result, characterization of NO variability is important in understanding the heat budget of the lower thermosphere. Finally, the descent of thermospheric NO is thought to be one of the ways in which the upper and lower atmosphere are coupled [*Solomon and Garcia*, 1984; *Garcia et al.*, 1984; *Siskind*, 2000]. NO, produced in the high-latitude lower thermosphere, can be transported to the stratosphere by the down-welling portion of the mean meridional circulation. Once in the stratosphere, it is relatively long-lived and can participate in catalytic reactions that destroy ozone. Consequently, stratospheric heating rates could be affected, and in so doing, it is thought that by this mechanism solar variability could drive variability in the lower atmosphere.

[3] Thermospheric NO typically has a peak concentration around 110 km. Concentrations are generally larger at high latitudes, where values of more than 2×10^8 molecules cm^{-3} are often observed. NO is produced primarily by the

0148-0227/04/2003JA010199

reaction of molecular oxygen and an excited nitrogen atom ($N(^2D)$):

$$N(^2D) + O_2 \rightarrow NO + O. \quad (1)$$

Sources of $N(^2D)$ include electron impact of molecular nitrogen and dissociative recombination of the NO^+ ion:

$$N_2 + e^* \rightarrow N(^2D) + N, \quad (2)$$

$$NO^+ + e \rightarrow N(^2D) + O. \quad (3)$$

Here e^* indicates energetic electrons, which are produced when precipitating particles (usually auroral electrons with characteristic energies of a few keV) or soft X rays interact with neutrals in the thermosphere. The flux of precipitating particles and soft X rays through the lower thermosphere varies dramatically with changes in solar activity, and so it follows that NO densities in that region of the atmosphere vary also. The strong degree of linkage between solar activity and NO is clearly seen in the satellite observations discussed earlier.

[4] This paper presents a three-dimensional nitric oxide empirical model (NOEM) based on eigenanalysis of SNOE satellite observations that parameterizes the spatial distribution of NO in the lower thermosphere in terms of proxies for different types of solar forcing. The model clearly characterizes the dominant modes of NO variability and provides insight into the causes of this variability.

2. Data Description

[5] The empirical model described here is derived solely from observations made by the SNOE satellite. SNOE was launched into a near-polar, Sun-synchronous, circular orbit in February 1998. A description of the satellite and instrumentation is provided by *Solomon et al.* [1996], and the ultraviolet spectrometer and methodology for observation of the (1,0) and (0,1) gamma bands is described by *Merkel et al.* [2001]. In the work of *Barth et al.* [2003], 935 days of global observations (from 11 March 1998 to 30 September 2000) were analyzed and showed clear correlations between observed NO and solar output. The analysis presented here is based on the same period, which spans much of the ascending phase of Solar Cycle 23. During this time, 10.7 cm solar radio flux (F10.7) varied from approximately 90 to 300 (in units of 10^{-22} W m^{-2} Hz^{-1}). Analysis is done on zonal mean daily averaged data (level 4) and restricted to an altitude range of 100 to 150 km because of possible contamination from polar mesospheric clouds at lower altitudes. The resolution of the data is 3.33 km in altitude and 5° in magnetic latitude and extends to ±82.5°. SNOE observations are almost fixed in local time over this observational period; all observations are within 30 min of 1045 hours. Since SNOE observes fluorescent scattering of solar radiation, no measurements are made during polar night. The data have been scaled to reflect a recent reevaluation of the fluorescent scattering g-factor (C. A. Barth and S. M. Bailey, Comparison of a thermospheric photochemical model with SNOE observations of nitric oxide, submitted to *Journal of Geophysical Research*, 2004). It should be noted that the empirical model described in the next section represents the atmosphere as observed by SNOE and therefore does not cover all local times or latitudes and will include any systematic errors in the original data set.

[6] Figure 1 shows the NO distribution derived from 2 days of observations. The large degree of variability of thermospheric NO is clearly apparent. In Figure 1a, NO densities on 22 October 1998 are enhanced at high latitudes when compared with observations on 30 March 2000. As will be shown in section 3, this indicates increased auroral production of NO. In contrast, the midlatitude densities are higher in the later observations and are an indication of enhanced soft X-ray fluxes associated with being closer in time to solar maximum.

3. Empirical Model

[7] Empirical orthogonal function (EOF) analysis is used to determine spatial structures in the SNOE data set that are capable of capturing the maximum amount of variance. EOF analysis, often used in climate research, is described by *van Storch and Zwiers* [1999, and references therein]. Generally, it is possible to represent any two-dimensional data set (i.e., data in space and time) as a time mean plus the sum of orthogonal functions of space multiplied by time-varying coefficients. Therefore the SNOE NO data set can be represented as

$$NO(y,z,t) = \overline{NO}(y,z) + \sum_i p_i(t) \cdot E_i(y,z). \quad (4)$$

$\overline{NO}$ is the time mean NO distribution, the coefficients p_i are usually referred to as principal components, and the functions E_i are empirical orthogonal functions (EOFs). For this analysis, the SNOE data are area weighted. EOFs are functions of geomagnetic latitude and height (y and z) and represent the spatial variability in the data set, while the principal components describe how this spatial variability varies in time. Typically, the EOFs are arranged in order of decreasing variance they can capture in the original data set. Table 1 lists the percentage variance captured by each of the first six EOFs derived from SNOE observations over 935 days. Taken together, the first three EOFs are able to explain almost 80% of the NO data set variance. The following three EOFs combined explain just an additional 8.8% of the total variance.

[8] The mean and first three EOFs are shown in Figure 2, while the first three principal components are shown in Figure 3. The normal convention of presenting EOFs in terms of physical units has been followed. Both EOFs and principal components have been scaled such that the variances of the principal component time series are unity. As is expected, the mean distribution shows distinct maxima at high latitudes, where NO is produced in the auroral regions as a consequence of particle precipitation. The first EOF appears to be associated with an enhancement in this aurorally produced NO. Its associated principal component follows the same high-frequency variability as the K_p planetary geomagnetic index, an indicator of auroral activity. K_p values were obtained from www.sec.noaa.gov and are shown in the upper portion of Figure 3a. The spatial

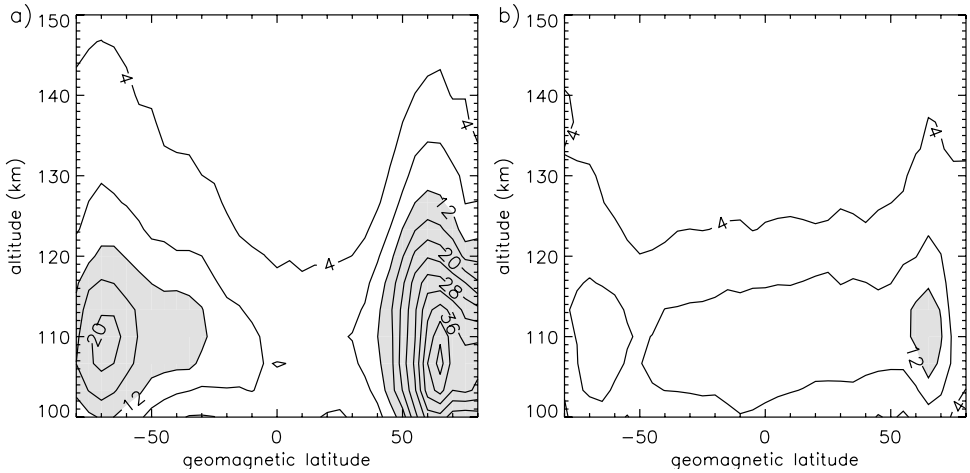

Figure 1. Observed NO distribution on (a) 22 October 1998 and (b) 30 March 2000. Contour intervals are every 4×10^7 cm^{-3}.

extent of the aurorally driven variability does not extend equatorward of 30° latitude. Variability in that region is manifest in the second and third EOFs.

[9] The second EOF pattern is asymmetric with respect to the equator, and inspection of the corresponding principal component suggests that it represents an annual variability that follows the solar declination angle (see Figure 3b). The timing of this variation is such that NO at high latitudes is diminished during summertime. The same seasonal variation was also seen by *Baker et al.* [2001]. The likely cause for such a variation is an increase in NO losses via the so-called "cannibalistic reaction":

$$NO + h\nu \rightarrow N + O \tag{5}$$

$$N + NO \rightarrow N_2 + O, \tag{6}$$

which results in a net loss of two NO molecules. Alternatively, this variation may also be caused by the sunlight suppression of discrete auroral arcs [*Newell et al.*, 1996]. The offset between geographic and magnetic poles is larger in the Southern Hemisphere than the Northern Hemisphere. As a consequence, more of the southern auroral oval is sunlit in winter. This could explain why the relative increase during wintertime at high latitudes is smaller in the Southern Hemisphere than the Northern Hemisphere.

[10] Finally, the third EOF reflects an enhancement in tropical NO. Its corresponding principal component shows both a long-term increase and high-frequency variability. Comparison with the F10.7 index (also obtained from www.sec.noaa.gov) indicates these changes are related to changes in solar output over the solar cycle and are due to solar rotation. F10.7 has been shown to correlate well with the 2–10 nm irradiance [*Bailey et al.*, 1999], and an enhancement in soft X rays will lead to increased energetic secondary electrons in the lower thermosphere and so increased NO production. Therefore the equatorial NO distribution is responding not only to the solar cycle but also to solar rotation. A similar response has been modeled by *Fuller-Rowell* [1993]. The third EOF shows an unexpected decrease at latitudes greater than 50° that also appears related to solar UV variability. A possible explanation is that this may again be related to an increase in the suppression of discrete auroral arcs as solar fluxes increase toward solar maximum. Alternatively, solar cycle induced variations in chemical composition or temperature of the lower thermosphere may be indirectly affecting NO production and loss and so the distribution of NO.

[11] While there is no guarantee that the modes of variability represented by the empirical orthogonal functions should be associated with physical phenomena, this is clearly the case for the first three EOFs. As is evident in Figure 3, their related principal components are highly correlated with the following geophysical parameters: K_p, solar declination (δ), and F10.7. The maximum correlation coefficients calculated between each principal component and the corresponding geophysical parameter range between 0.65 and 0.88 and are listed in Table 2, along with the lag in days at which the maximum occurred. The maximum correlations occur in principal components 1 and 3 with a lag of 1 day from the time series of the solar proxies. In other words, it takes about a day for NO to respond to changes in solar forcing. This is similar to the finding of *Solomon et al.* [1999], who compared averages of NO over latitude ranges with these proxies and found the 1 day lag consistent with the chemical lifetime for NO in the lower thermosphere.

[12] Typically, attribution of a geophysical driver for anything but the first EOF is problematic. EOF analysis ensures that the lag-0 cross-correlations of all principal components be zero, and so if the geophysical drivers are in some way correlated, then their related effects will not project onto different EOFs. For the SNOE data, the modes

Table 1. Summary of Variances Captured From the SNOE Data Set by the First Six Empirical Orthogonal Functions (EOFs)

EOF	% Variance	Cumulative % Variance
1	45.2	45.2
2	21.4	66.6
3	12.4	79.0
4	4.0	83.0
5	2.9	85.9
6	1.9	87.8

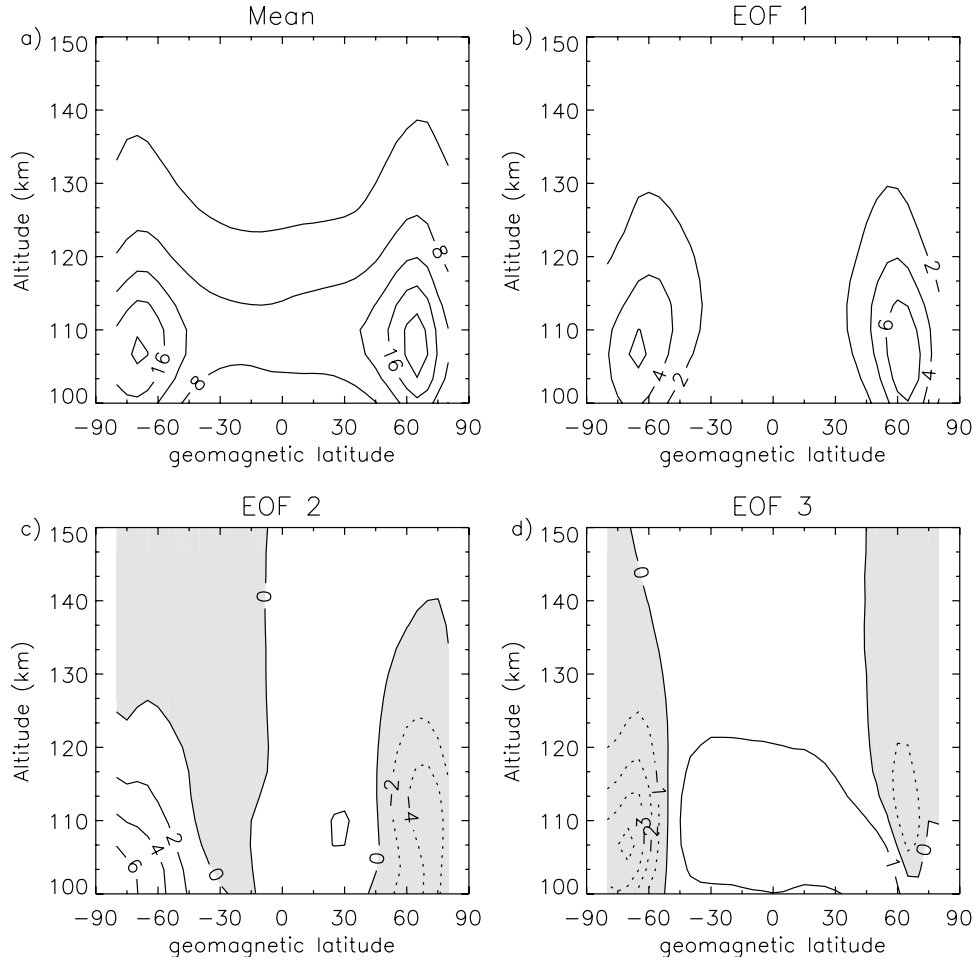

Figure 2. Mean number density (10^7 cm^{-3}) and first three empirical orthogonal functions derived from the SNOE NO data set.

of variability described by the second and third EOFs do appear related to separate geophysical phenomena. However, it should be remembered that these EOFs are subject to the additional constraint that all EOFs be orthogonal to each other. Interestingly, the use of orthogonal functions appears to have been successful in analyzing SNOE NO data because the geophysical drivers are not highly correlated over the period of SNOE observations. For example, while it is commonly thought that during solar maximum, solar storms and subsequent auroral activity are more frequent [*Papitashvili et al.*, 2000], the cross-correlation coefficient between daily F10.7 and daily K_p is just 0.14 between 1998 and 2000 (the cross-correlation increases if the K_p data are smoothed and a longer time period is considered). The cross-correlation coefficient is not zero, however, and this might provide yet another explanation for the high-latitude minima in EOF 3 (Figure 2d).

[13] In Figure 4, principal component values for each day are plotted against their related geophysical parameter shifted in time according to the lags listed in Table 2. To generalize the model for a variety of geophysical conditions, the principal components are replaced with least squares polynomial fits (f_i) plotted as solid lines in Figure 4. One advantage of using F10.7 and K_p is that these parameters are readily available and often used as input into existing empirical models (e.g., the thermospheric model of *Hedin* [1991]). Expressions for these polynomial fits are listed in Table 3. A linear fit was chosen for f_1, since nitric oxide production should vary proportionately with auroral energy input (which itself is proportional to K_p [*Maeda et al.*, 1989]). A better fit was achieved if the logarithm of F10.7 was used for f_3, which is again consistent with the modeled response of equatorial NO to the solar cycle flux variation (see Figure 9 of *Fuller-Rowell* [1993]). If only the first three EOFs are retained and the derived polynomial fits are used in place of the principal components time series, equation (4) is simplified to

$$NO(y,z,t) = \overline{NO}(y,z) + f_1\left(K_p\right)\cdot E_1 + f_2(\delta)\cdot E_2 + f_3(F10.7)\cdot E_3. \tag{7}$$

Model parameters are calculated on the day indicated by the lag parameter in Table 2. Declination is calculated using the formulation of *Paltridge and Platt* [1976].

[14] Two examples of the model-created zonal mean NO distribution for differing geophysical conditions (corresponding to the same conditions in Figure 1) are shown in Figure 5. The empirical model predictions reproduce the large-scale features for each day. The input K_p indices for these modeled distributions were 3.5 and 1.6 for

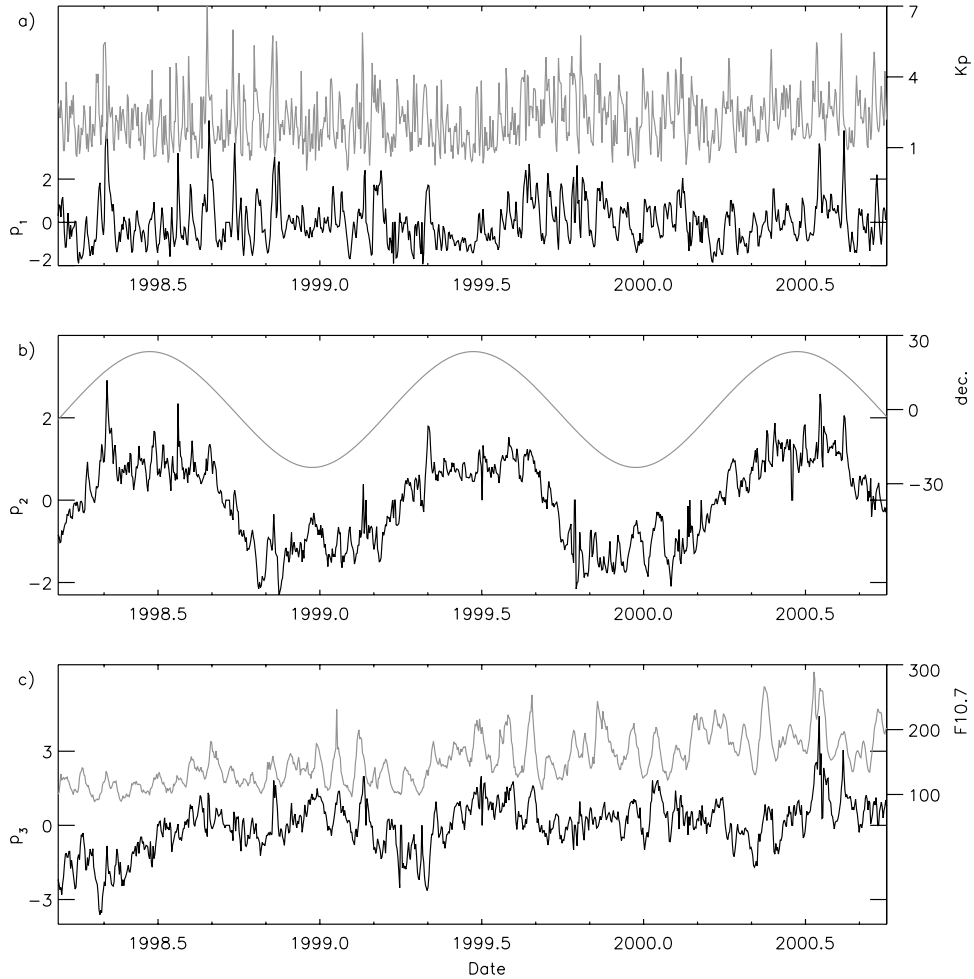

Figure 3. Time variation in first three principal components (dark lines and axes on left-hand side of figures). Associated geophysical parameters (K_p, declination, and F10.7) are shown as light lines with values according to axes on right-hand side of figures.

Figures 5a and 5b, respectively. These were the average values for the days preceding the observations in Figure 1. On 22 October 1998 the empirical model predicts enhanced NO in the auroral regions, a consequence of a larger contribution from EOF 1. In contrast, the contribution from EOF 3 (and so midlatitude NO) is larger in the simulation for 30 March 2000 because the F10.7 index used is almost double that used for the earlier simulation (208 versus 117). Figure 6 shows an 18 month time series of SNOE nitric oxide observations near the lower thermospheric maximum (106.7 km), as well as model simulations based on observed geophysical conditions. The figure illustrates that the model is capable of reproducing much of the variability (both short-term and long-term) in the observations.

[15] Since the correlations between parameter and principal component are not unity, the model based on geophysical parameters does not capture the same level of variance in the original data as one based on the original principal components. The percentage variance captured by the empirical model based on equation (7) is

$$\left(1 - \frac{var(NO_{obs} - NO_{mod})}{var(NO_{obs})}\right) \times 100, \qquad (8)$$

where NO_{obs} are observations and NO_{mod} are model predictions. Over all 935 days of SNOE observations the model is capable of capturing 50.2% of the variance in the observations. Using higher-order polynomials for f_1 and f_3 did not increase the percentage of the variance captured. Considering that the first three EOFs and principal components were able to capture 79.0%, the lower percentage may appear unsatisfactory. However, at least some of the variance not captured represents geophysical or measurement noise unrelated to the processes outlined above. In addition, the empirical model has the advantage that it allows predictions for conditions not reproduced in the SNOE data set, and it is considerably smaller in size.

[16] The spatial distribution of the average differences between the empirical model and the entire SNOE data set

Table 2. Correlation Coefficients for First Three EOFs With Geophysical Parameters

EOF	Correlated Parameter	Correlation Coefficient	Lag, days
1	Kp	0.776	1
2	declination (δ)	0.884	0
3	$\log_{10}(F10.7)$	0.654	1

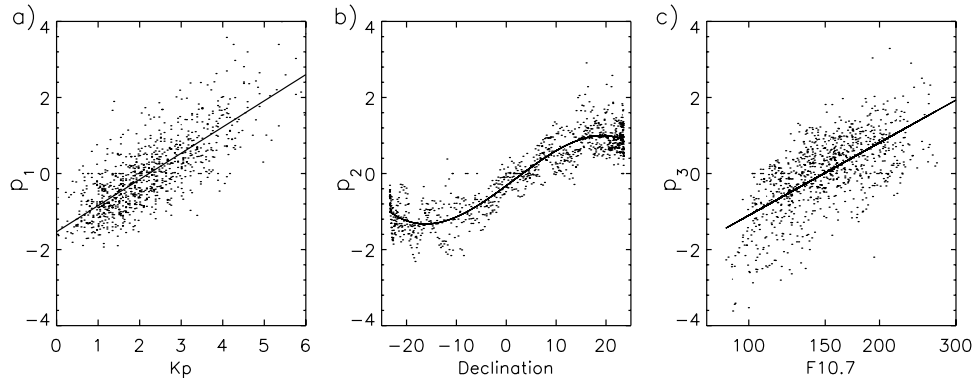

Figure 4. Scatter plots of (a) daily average Kp versus principal component 1 (p_1), (b) declination versus p_2, and (c) F10.7 versus p_3. Solar indices from www.sec.noaa.gov.

is shown in Figure 7a. Typically, the average values calculated from the model agree with observations to within 2%. The standard deviations of the relative differences are shown in Figure 7b. Within the tropics the standard deviations are in the range 0.16 to 0.27 for all heights. At the locations of the NO maxima in the auroral zones the standard deviations are approximately 0.3 and, as might be expected, more than two-thirds of the observations fall within 30% of the model predictions.

[17] Also shown in Figure 6 are observations of NO at 106.7 km made by the Halogen Occultation Experiment (HALOE) on board the Upper Atmosphere Research Satellite [*Russell et al.*, 1993]. HALOE data are daily averages of version 19 data that fall within 2.5° of the indicated magnetic latitude bands. Data are only shown if more than one profile fell within the latitude band on a given day. Since HALOE is a solar occultation experiment, on a satellite whose orbit is slowly precessing, sunrise and sunset occultations at a particular magnetic latitude occur approximately once per month (or less if the instrument is not operated continuously). However, where HALOE observations are available, they appear to be in good agreement with both SNOE observations and the empirical model. Differences that do exist between the data sets could be due in part to the differing local times of the observations (HALOE observations occurring at sunrise and sunset, while SNOE is a approximately 1045 hours local time).

[18] If the empirical model is to be used to either constrain or validate a global circulation model it is usually necessary to transform the predicted zonal mean NO distribution (in geomagnetic coordinates) to a three-dimensional geographic distribution. This is done using the eccentric dipole coordinate transformation of *Fraser-Smith* [1987]. An example of the transformed NO distributions for four consecutive days beginning on 19 August 1998 are shown in Figure 8, along with SNOE observations. Unlike the geomagnetic zonal mean SNOE data set used to derive the empirical model, the SNOE data in Figure 8 are interpolated onto a constant latitude/longitude grid from individual NO profile measurements taken over each day.

[19] Even over such a small time period, the high degree of variability in NO concentrations is apparent, with a doubling or more seen in both model and observations. The primary driver of model variability is the factor of 5 increase in the K_p index (F10.7 and declination are practically constant over the period). The three-dimensional distributions highlight the utility of performing the EOF analysis in geomagnetic coordinates. Observations show a large degree of zonal asymmetry (in geographic coordinates) that is the result of nitric oxide production in the aurora that is aligned along geomagnetic longitude circles. This asymmetry is most apparent in the Southern Hemisphere where the offset between geographic and geomagnetic poles is larger than the Northern Hemisphere. Using the empirical model, the effects of geographic zonal asymmetry in NO distribution can now be considered in three-dimensional models. It remains to be seen if results from such models will vary significantly from their two-dimensional predecessors.

4. Conclusion

[20] NOEM, an empirical model of nitric oxide in the lower thermosphere (100–150 km) has been constructed based on over 2.5 years of SNOE observations using the method of empirical orthogonal functions. The model is capable of capturing a large amount of the variance in the observations, which has been associated with three geophysical forcing parameters (in decreasing order of importance): (1) auroral forcing, (2) changes in solar declination (or, equivalently, the day of year), and (3) solar soft X-ray flux variations. The spatial extent of the NO response to these forcings is clearly defined in the model and allows examination of the relative roles of aurora and soft X rays in NO production. By replacing the principal components with fitted functions of solar proxies, the model has been extended to cover a wide range of geophysical conditions.

[21] In the work of *Siskind* [2000], there is a call for the use of three-dimensional models to study how transport of NO can couple the thermosphere and stratosphere. The models used in such studies will necessarily need to include many complex processes to model the extended altitude

Table 3. Polynomial Expressions for Solid Curves Shown in Figure 4

Curve	Expression
a	$f_1(K_p) = 0.689 \cdot K_p - 1.53$
b	$f_2(\delta) = -1.04 \cdot 10^{-4} \cdot \delta^3 + 4.90 \cdot 10^{-4} \cdot \delta^2 + 0.0973 \cdot \delta - 0.320$
c	$f_3(F10.7) = 6.36 \cdot \log_{10}(F10.7) - 13.8$

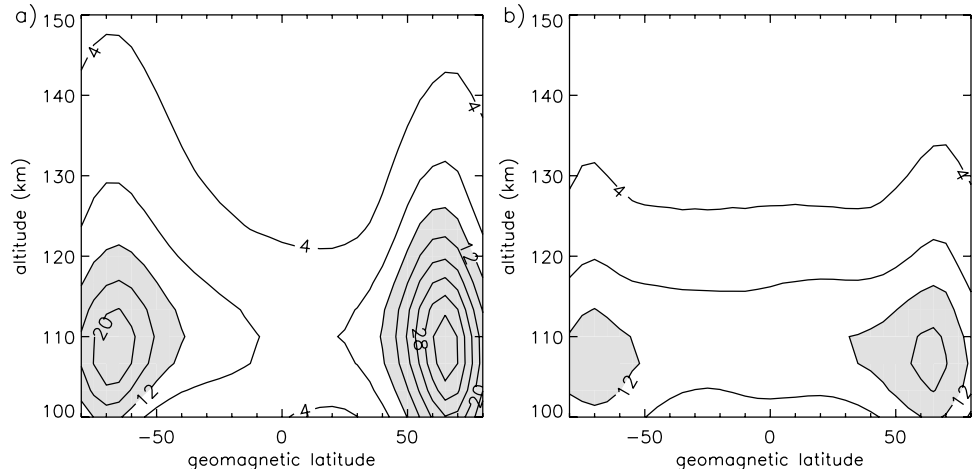

Figure 5. Empirical estimates of NO number densities on the same days as Figure 1. Contour intervals are every 4×10^7 cm^{-3}.

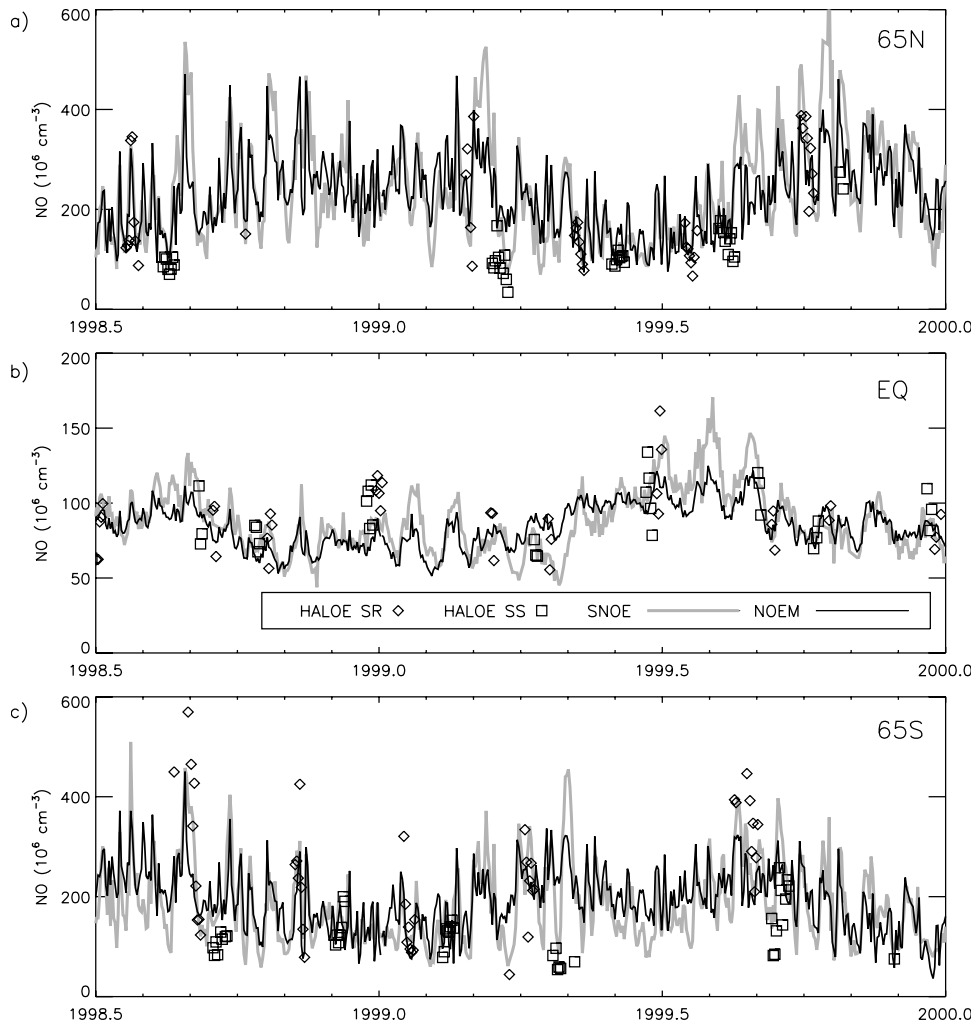

Figure 6. Observed and modeled daily mean nitric oxide concentrations at 106.7 km for the period between 1 July 1998 and 31 December 2000. Observations are based on averages of profiles that were within 2.5° of (a) 65°N, (b) 0°, and (c) 65°S magnetic latitude. See color version of this figure at back of this issue.

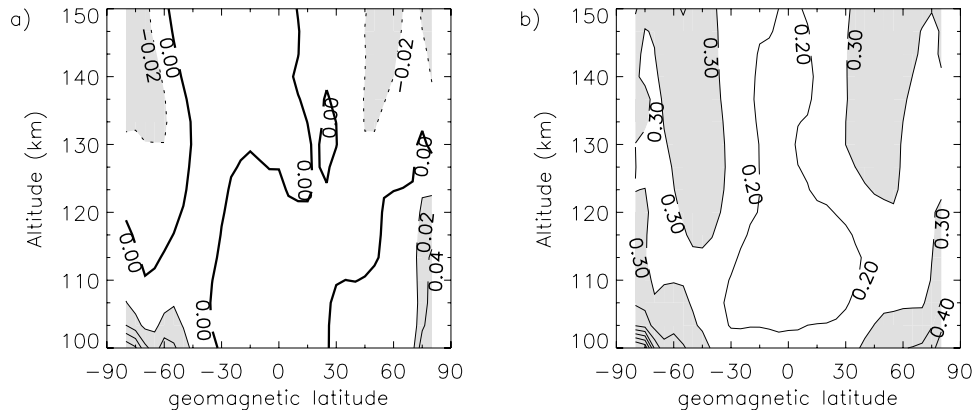

Figure 7. (a) Relative differences (*obs./model* − 1) between SNOE observations and the empirical model averaged over all available data. Shaded regions are for differences with magnitude larger then 0.02. (b) Standard deviation of relative differences calculated in Figure 7a. Shaded regions are for regions greater then 0.3.

range. The empirical model described above should prove useful in providing validation of thermospheric NO densities in these extended models. Alternatively, by constraining general circulation models with empirical NO densities over a variety of solar conditions, the extent to which stratospheric composition is affected by variations in thermospheric NO densities could be tested. It is worth repeating that the model is based solely on SNOE observations and its use in such studies should consider the conditions under which those observations were made. Source code and EOF data necessary to run NOEM can be obtained by contacting the authors.

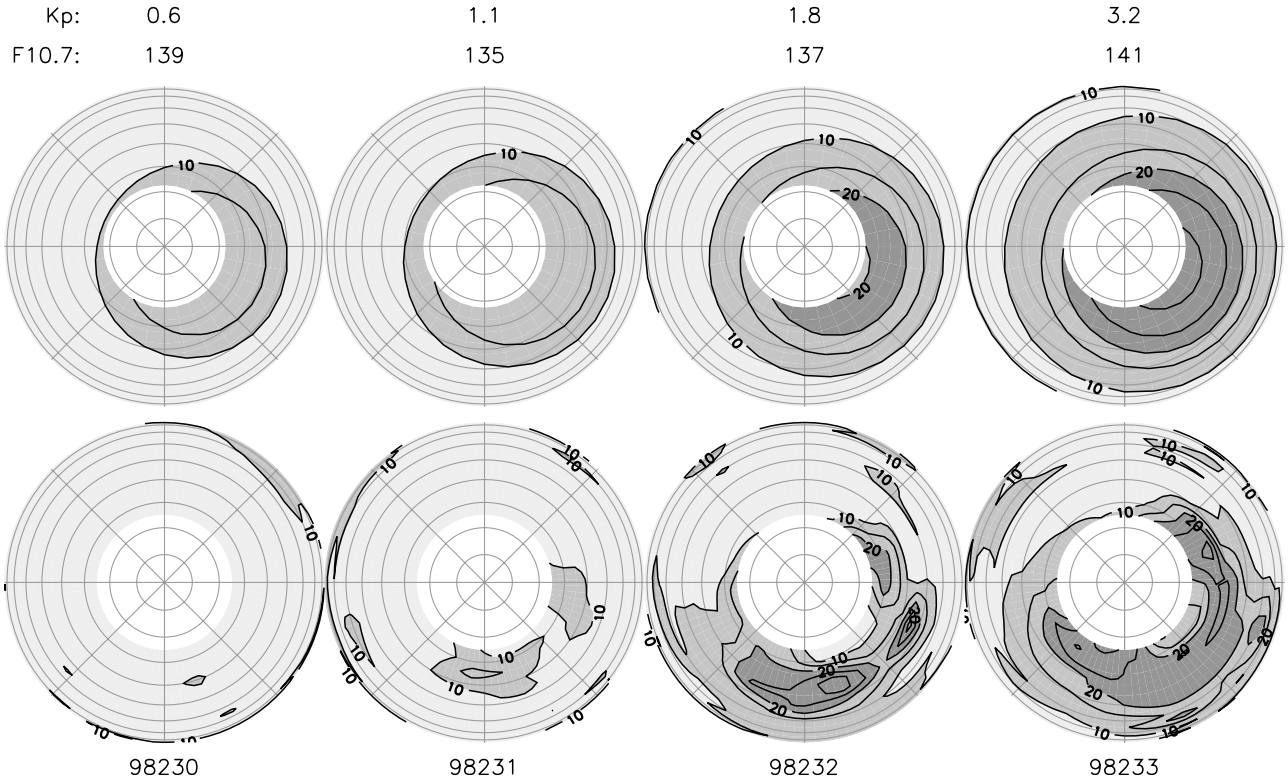

Figure 8. A comparison between modeled (top) and observed (bottom) Southern Hemispheric NO distributions at 110 km for four consecutive days beginning on 19 August 1998. Zero longitude is at the top of each plot, which extends from the equator to the south pole. Model predictions are calculated using K_p and F10.7 listed at the top of the figure and are averages over the previous day. Observed distributions are interpolated onto a uniform grid from approximately 15 orbits of SNOE data. Model predictions are masked where no observations were made.

[22] **Acknowledgments.** Support for this work was provided by NASA Office of Space Science. The National Center for Atmospheric Research is operated by the University Corporation for Atmospheric Research under sponsorship of the National Science Foundation.

[23] Shadia Rifai Habbal thanks Jean-Claude Gerard and another referee for their assistance in evaluating this paper.

References

Bailey, S. M., T. N. Woods, C. A. Barth, and S. C. Solomon (1999), Measurements of the solar soft X-ray irradiance from the Student Nitric Oxide Explorer, *Geophys. Res. Lett.*, *26*, 1255–1258.

Baker, D. N., C. A. Barth, K. E. Mankoff, S. G. Kanekal, S. M. Bailey, G. M. Mason, and J. E. Mazur (2001), Relationships between precipitating auroral zone electrons and lower thermospheric nitric oxide densities: 1998–2000, *J. Geophys. Res.*, *106*, 24,465–24,480.

Barth, C. A. (1996), Reference models for thermospheric nitric oxide, 1994, *Adv. Space Res.*, *18*, 179.

Barth, C. A., W. K. Tobiska, D. E. Siskind, and D. D. Cleary (1988), Solar-terrestrial coupling: Low-latitude thermospheric nitric oxide, *Geophys. Res. Lett.*, *15*, 92–94.

Barth, C. A., S. M. Bailey, and S. C. Solomon (1999), Solar-terestrial coupling: Solar soft X rays and thermospheric nitric oxide, *Geophys. Res. Lett.*, *26*, 1251–1254.

Barth, C. A., K. D. Mankoff, S. M. Bailey, and S. C. Solomon (2003), Global observations of nitric oxide in the thermosphere, *J. Geophys. Res.*, *108*(A1), 1027, doi:10.1029/2002JA009458.

Fraser-Smith, A. C. (1987), Centered and eccentric geomagnetic dipoles and their poles, 1600–1985, *Rev. Geophys.*, *25*, 1–16.

Fuller-Rowell, T. J. (1993), Modeling the solar cycle change in nitric oxide in the thermosphere and upper atmosphere, *J. Geophys. Res.*, *98*, 1559–1570.

Garcia, R. R., S. Solomon, R. G. Roble, and D. W. Rusch (1984), A numerical response of the middle atmosphere to the 11-year solar cycle, *Planet. Space Sci.*, *32*(4), 411–423.

Gerard, J. C., C. G. Feen, and D. W. Rusch (1990), Solar cycle variation of thermospheric nitric oxide at solstice, *J. Geophys. Res.*, *95*, 12,235.

Hedin, A. E. (1991), Extension of the MSIS thermosphere model into the middle and lower atmosphere, *J. Geophys. Res.*, *96*, 1159–1172.

Maeda, S., T. J. Fuller-Rowell, and D. S. Evans (1989), Zonally averaged dynamical and compositional response of the thermosphere to auroral activity during September 18–24, 1984, *J. Geophys. Res.*, *94*, 16,869–16,883.

Merkel, A. W., C. A. Barth, and S. M. Bailey (2001), Altitude determination of ultraviolet measurements made by the Student Nitric Oxide Explorer, *J. Geophys. Res.*, *106*, 30,283–30,290.

Newell, P. T., C.-I. Meng, and K. M. Lyons (1996), Suppression of discrete aurorae by sunlight, *Nature*, *381*, 766–767.

Paltridge, G. W., and C. M. R. Platt (1976), *Radiative Processes in Meteorology and Climatology*, pp. 62–63, Elsevier Sci., New York.

Papitashvili, V. O., N. E. Papitashvili, and J. H. King (2000), Solar cycle effects in planetary geomagnetic activity: Analysis of 36-year long OMNI dataset, *Geophys. Res. Lett.*, *27*, 2797–2800.

Richards, P. G., M. R. Torr, and D. G. Torr (1982), The seasonal effect of nitric oxide cooling on the thermospheric u.v. heat budget, *Planet. Space. Sci.*, *30*(5), 515–518.

Russell, J. M., III, et al. (1993), The Halogen Occultation Experiment, *J. Geophys. Res.*, *98*, 10,777–10,797.

Siskind, D. E. (2000), On the coupling between middle and upper atmospheric odd nitrogen, in *Atmospheric Science Across the Stratopause*, *Geophys. Monogr. Ser.*, vol. 123, edited by D. E. Siskind, S. D. Eckermann, and M. E. Summers, pp. 101–116, AGU, Washington, D. C.

Siskind, D. E., C. A. Barth, and R. G. Roble (1989a), The response of thermospheric nitric oxide to an auroral storm: 1. Low and middle latitudes, *J. Geophys. Res.*, *94*, 16,885.

Siskind, D. E., C. A. Barth, D. S. Evans, and R. G. Roble (1989b), The response of thermospheric nitric oxide to an auroral storm: 2. Auroral latitudes, *J. Geophys. Res.*, *94*, 16,899.

Solomon, S. C., and R. R. Garcia (1984), Transport of thermospheric NO to the upper stratosphere?, *Planet. Space. Sci.*, *32*(4), 399–409.

Solomon, S. C., et al. (1996), The Student Nitric Oxide Explorer, *SPIE*, *2810*, 121.

Solomon, S. C., C. A. Barth, and S. M. Bailey (1999), Auroral production of nitric oxide measured by the SNOE satellite, *Geophys. Res. Lett.*, *26*, 1259–1262.

van Storch, H., and F. W. Zwiers (1999), *Statistical Analysis in Climate Research*, Cambridge Univ. Press, New York.

D. R. Marsh and S. C. Solomon, National Center for Atmospheric Research, P.O. Box 3000, Boulder, CO 80307-3000, USA. (marsh@ucar.edu; stans@ucar.edu)

A. E. Reynolds, Department of Meteorology, Pennsylvania State University, University Park, PA 16802, USA. (aer149@ucar.edu)

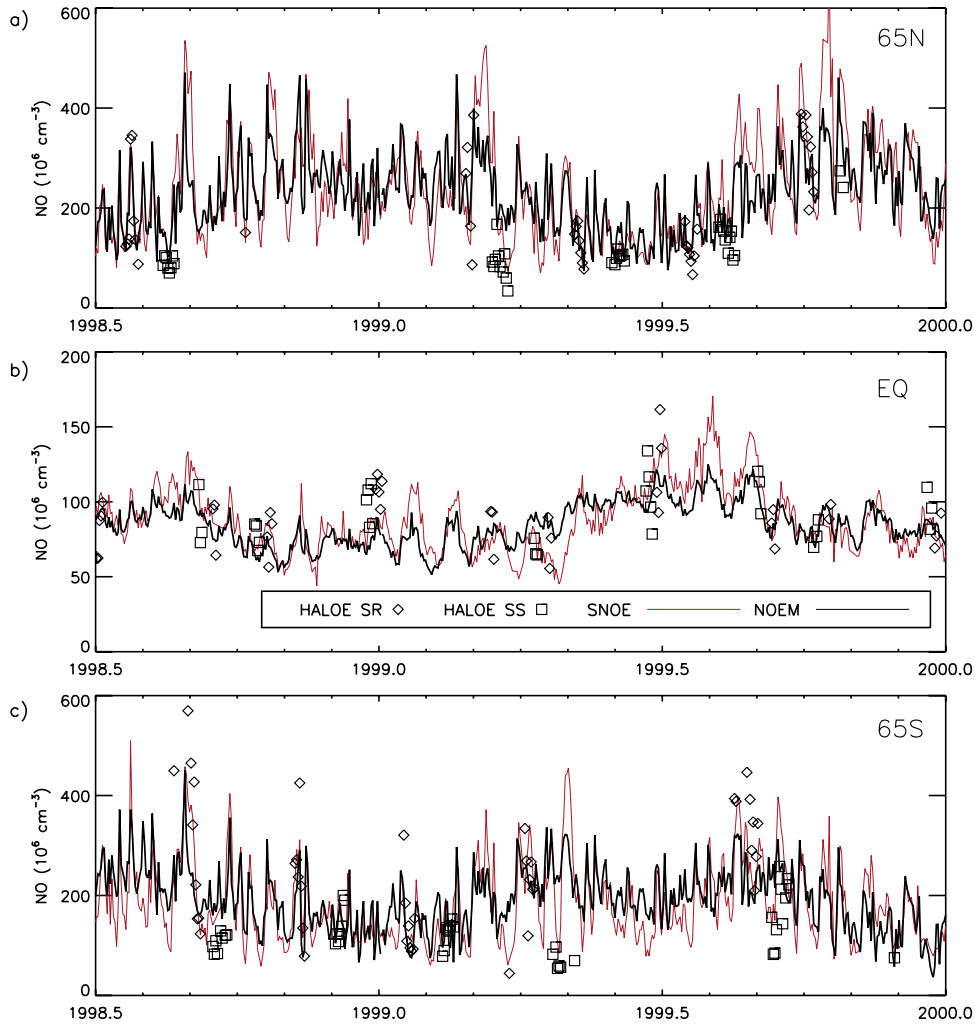

Figure 6. Observed and modeled daily mean nitric oxide concentrations at 106.7 km for the period between 1 July 1998 and 31 December 2000. Observations are based on averages of profiles that were within 2.5° of (a) 65°N, (b) 0°, and (c) 65°S magnetic latitude.